Supporting Information

Origins of the Instability of Non-precious HER Catalysts at Open Circuit Potential

Zhenbin Wang,[1,†] Ya-Rong Zheng,[1,3,†] Joseph Montoya,[2] Degenhart Hochfilzer,[1] Ang Cao,[1] Jakob Kibsgaard,[1] Ib Chorkendorff,[1] and Jens K. Nørskov,[1,*]

[1]Department of Physics, Technical University of Denmark, 2800 Kongens Lyngby, Denmark

[2]Toyota Research Institute, Los Altos, CA 94022, USA

[3]Anhui Province Key Laboratory of Advanced Catalytic Materials and Reaction Engineering, School of Chemistry and Chemical Engineering, Hefei University of Technology, 230009, Hefei, China.

[†]These authors contributed equally

E-mail: jkno@dtu.dk

Computational Methods

Density functional theory

All density functional theory (DFT) calculations were performed using Vienna *ab initio* simulation package within the projector-augmented wave method.[1,2] The strongly constrained and appropriately normed (SCAN) functional[3] was used for the exchange-correlation description. The plane wave energy cutoff was set to 520 eV. The electronic energy and atomic forces were converged to within 10^{-5} eV and 0.02 eV/Å. The Brillouin zone was sampled with a *k*-point density of at least 1000 per reciprocal atom.[4] All calculations were spin-polarized. The crystal structure manipulations and data analysis were carried out using the Pymatgen software package.[5]

Pourbaix diagram

Methodologies of Pourbaix diagram construction based on DFT calculations have been detailed in prior works.[6–9] The basic principles are summarized as below. In the Pourbaix diagram construction, the stable domains are determined based on the knowledge of all possible equilibrium redox reactions in the chemical space of interest.

In an aqueous solution under certain pH ($-log[\mathrm{H^+}]$) and potential (E), the following redox reaction takes place:

$$[Reactants] + \mathrm{H_2O} \Leftrightarrow [Products] + m\mathrm{H^+} + n\mathrm{e^-} \tag{1}$$

At equilibrium, the Gibbs free energy change (ΔG_{rxn}) of this reaction can be related to E using the Nernst equation:

$$-nFE = \Delta G_{\mathrm{rxn}} = \Delta G^{o}_{\mathrm{rxn}} + 2.303 \times RT \times log\frac{a_{Reactants}}{a_{Products}} - 2.303 \times RT \times m \times \mathrm{pH} \tag{2}$$

where $\Delta G^{\mathrm{o}}_{\mathrm{rxn}}$ is the Gibbs free energy change of the reaction at standard conditions, F is the Faraday constant, R is the gas constant, and T is the temperature. a is the activity. The most stable species in aqueous solutions can be therefore determined by minimizing ($\Delta G_{\mathrm{rxn}} + nFE$) across all possible

reactions under certain pH and applied potential (E). The aqueous stability of a catalyst could be quantitatively estimated by its chemical potential difference (ΔG_{pbx}) with respect to the stable domains on the Pourbaix diagram under working conditions. Note that the zero-point energy and integrated heat capacity for both solids and gases are neglected by assuming the differences in these quantities between reactants and products are negligible at room temperature.[9] The chemical potentials of solids and aqueous ions are provided in Table S3. The raw data (structures and energies) are shared via **figshare**.

Experimental Methods

Exfoliation of commercial MoS_2

Typically, 500 mg commercial MoS_2 (Fluka, CAS no.: 1317-33-5) was mixed with 40 mL N,N-Dimethylformamide (DMF, CAS no. 68-12-2) and sonicated continuously for 8 hours. The resultant solution was centrifuged at 2,000 rpm for 10 min, and the supernatant was further centrifuged at 15,000 rpm for 20 min to obtain the exfoliated MoS_2. The resultant sample was washed several times by ethanol.

Preparation of CoP

The CoP was prepared by a two-step method. First, Co-O-H precursor was prepared by mixing 1 M Co^{2+} and 2 M OH^- solution with mechanical stirring under ambient conditions. The precipitate was centrifuged at 6,000 rpm for 5 min, and was washed several times by ethanol and Milli-Q (18 Mω cm^{-1}) water, the precursor was dried under at 100 °C for 6 h. After that, 100 mg dried Co-O-H precursor and 2 g $NaH_2PO_2{\cdot}H_2O$ (Aldrich, CAS no.: 7681-53-0) were placed at two separated positions in a ceramic boat with the $NaH_2PO_2{\cdot}H_2O$ at the upstream side. With a heating rate of 10 °C min^{-1}, the samples were heated at 400 °C for 30 min in Ar atmosphere.

Preparation of MoP

Typically, 2.7821 g of $(NH_4)_6Mo_7O_{24}{\cdot}4H_2O$ (Fluka, CAS no.: 12054-85-2) and 2.0797 g of (NH4)2HPO4 (Aldrich, CAS no.: 7783-28-0) were dissolved in 6 mL of H_2O, the solution was evaporated at 90 °C for 2 h under 200 rpm and then dried at 120 °C for 2 days. Finally, the Mo-P precursor was heated to 665 °C with a heating rate of 1 °C min^{-1}, and held for 2 h under H_2 stream with a flow rate of 116 mL min-1 to get the final MoP.

Characterization (XRD, XPS, ICP-MS)

Phase structure of the prepared material was determined by X-ray diffraction (XRD) using a PANalytical Empyrean diffractometer with Cu Kα radiation (λ = 1.54178 Å). The concentration of dissolved metal iones were detected using inductively coupled plasma-mass spectrometry (ICP-MS, Fischer Scientific, model iCAP-QC ICP-M).

Electrochemical measurements

All the electrochemical measurements were conducted in a three electrodes setup with a H-cell configuration at ambient temperature, as previously described in Ref 10. A $Hg/HgSO_4$ electrode and a graphite rod were used as the reference and counter electrodes, respectively. A rotating disk electrode with glassy carbon (PINE, 0.196 cm^2) was used as the working electrode. All the electrodes were connected to a Multipotentiostat (VMP2, Biologic). The potentials reported here were normalized versus the reverse hydrogen electrode by measuring the open circuit potential (OCP) at a Pt electrode in H_2-saturated electrolyte. To make the catalyst ink, 4 mg catalyst powder was dispersed in 1 mL of 1:3 v/v isopropanol/DIW mixture with 40 μL Nafion solution (5 wt%), which was ultrasonicated to obtain a homogeneous ink. Then, 20 μL catalyst ink was pipetted onto the glassy carbon electrode with a loading of $\sim$0.4 mg cm^{-2}. The polarization curves were obtained by sweeping the potentials from -0.7 to 0 versus RHE with a scan rate of 20 mVs^{-1} and 1600 rpm in H_2-saturated 0.5 M H_2SO_4 solution at ambient temperature. The corrosion measurements were

performed by chronoamperometry at different potentials. ICP-MS was employed to analyze the dissolved metal ions during chronopotentiometry. Each ICP-MS data point was collected at least three times.

MP-PBE Mo-S Pourbaix diagram

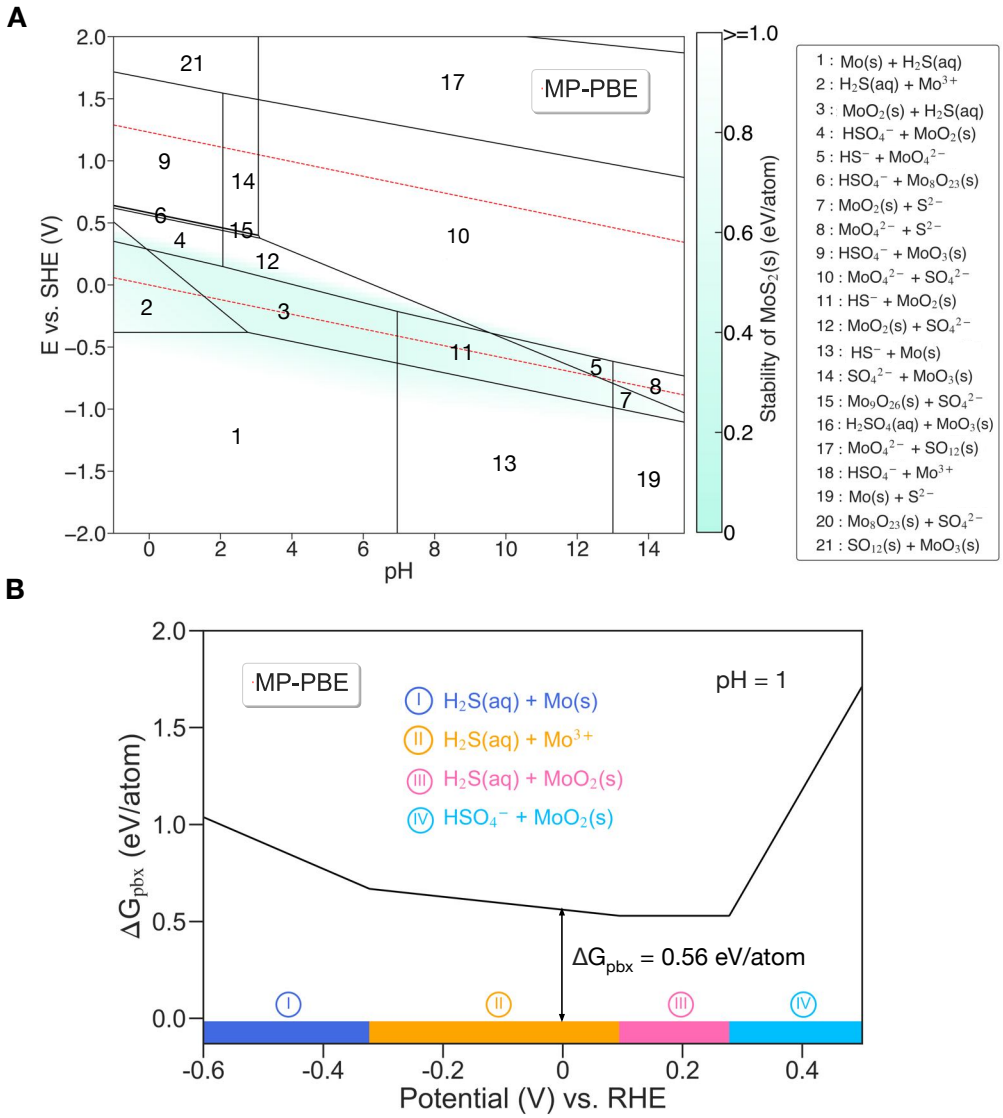

Figure S1: (A) The Materials Project PBE (MP-PBE) calculated Mo-S Pourbaix diagram generated with aqueous ion concentration of 10^{-6} M at 25°C. The Lake blue color measures the stability of MoS_2 at relevant potential and pH. The water stability window is shown in red dashed line. (B) Calculated decomposition free energy (ΔG_{pbx}) of MoS_2 from the potential -0.6−0.5 V *vs*. RHE at pH = 1. The projection of ΔG_{pbx} onto the potential axis highlights the stable species at the corresponding regions.

MoS_2 does not appear in the MP-PBE calculated Mo-S Pourbaix diagram (Figure S1A), suggesting that it might be unstable or metastable. Based on Figure S1A, we quantitatively analyzed the stability of MoS_2 by calculating its ΔG_{pbx} from potential of -0.6 V to 0.5 V at pH = 1, shown in

Figure S1B. The MP-PBE calculated ΔG_{pbx} of MoS_2 is higher than 0.57 eV/atom when the potential is lower than 0 V, implying that MoS_2 would experience a very large thermodynamic driving force to decompose during electrocatalysis. This predicted instability of MoS_2 under typical hydrogen evolution potentials is inconsistent with experiment.[11–14]

Mo-P Pourbaix diagram

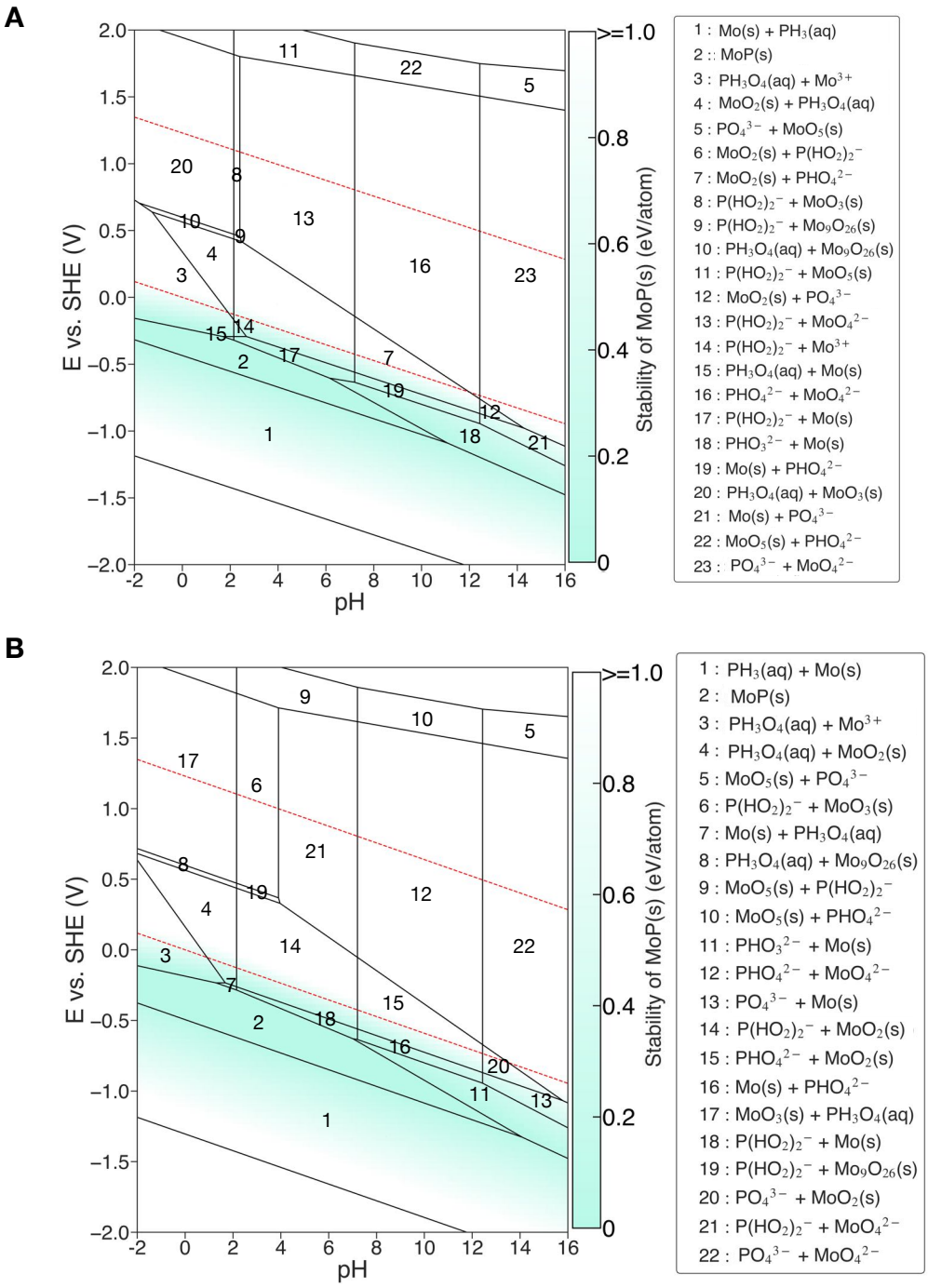

Figure S2: SCAN-calculated Mo-P Pourbaix diagrams generated with aqueous ion concentration of (A) 10^{-6} M and (B) 10^{-3} at 25°C. The blue color measures the stability of MoP at relevant potential and pH. The deeper the blue, the more stable of MoP. The water stability window is shown in red dashed line.

Co-P Pourbaix diagram

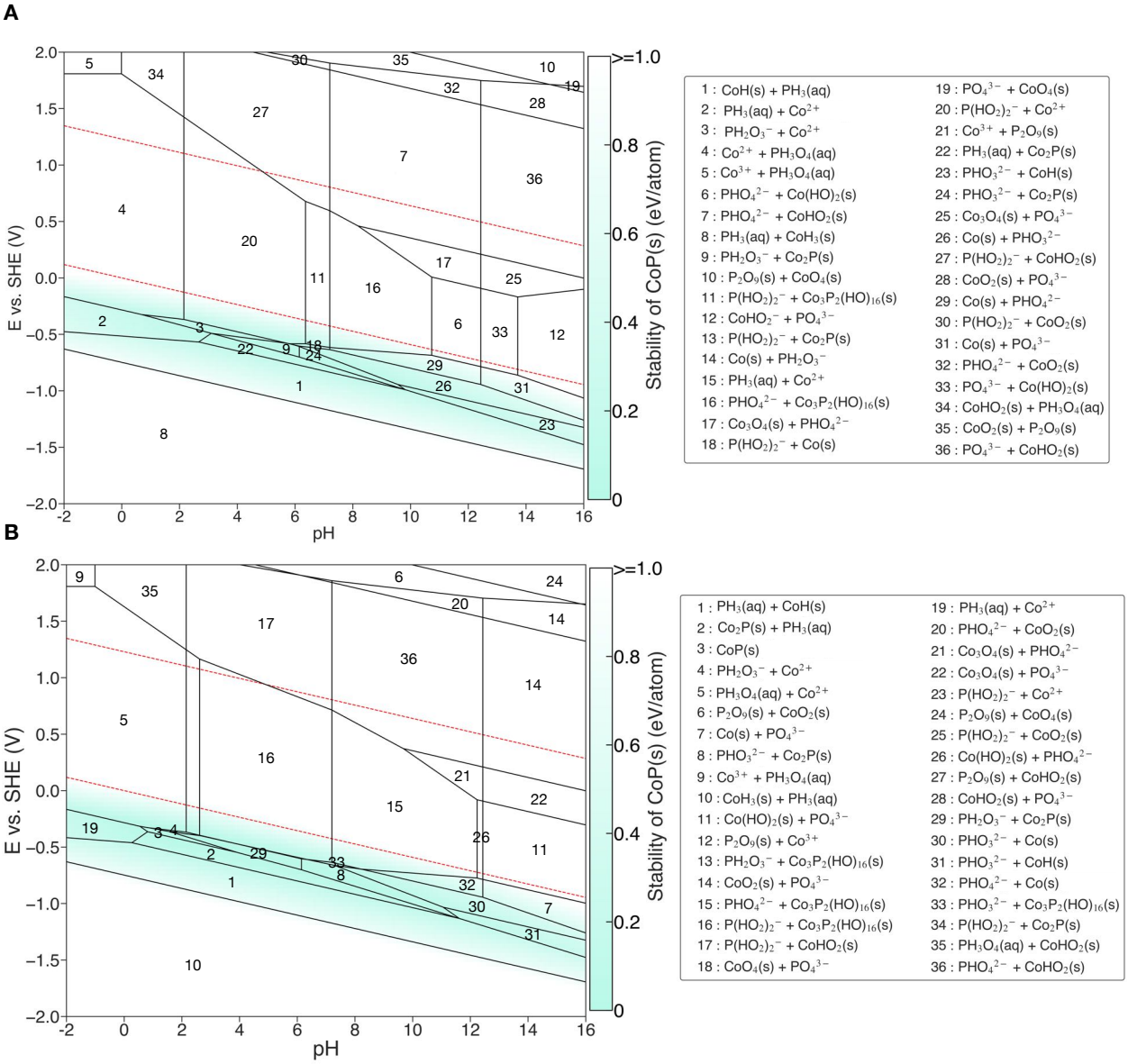

Figure S3: SCAN-calculated Co-P Pourbaix diagrams generated with aqueous ion concentration of (A) 10^{-6} M and (B) 10^{-3} at 25°C. The blue color measures the stability of CoP at relevant potential and pH. The water stability window is shown in red dashed line.

Pt Pourbaix diagram

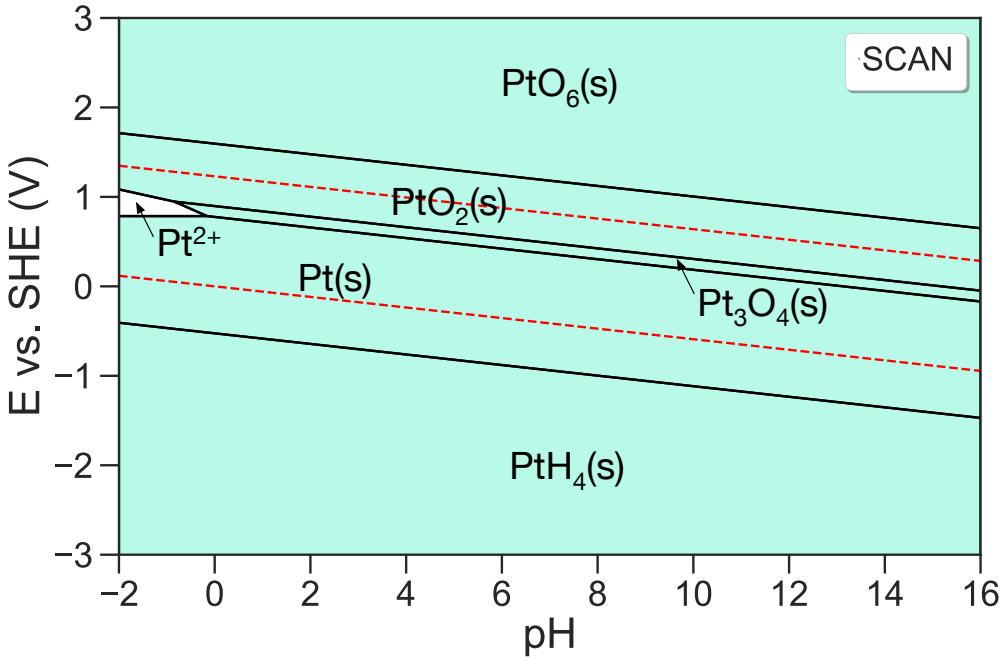

Figure S4: SCAN-calculated Pt Pourbaix diagrams generated with aqueous ion concentration of 10^{-6} M at 25°C. Regions with solid are shaded in Lake blue. The water stability window is shown in red dashed line.

Compared to the experimental Pt Pourbaix diagram reported in Ref 15, we note that $Pt(OH)_2$ does not appear on this calculated diagram. This is because $Pt(OH)_2$ is not considered in the Pourbaix diagram calculation due to the missing data on its crystal structure in the literature.

Formation enthalpies of phosphides

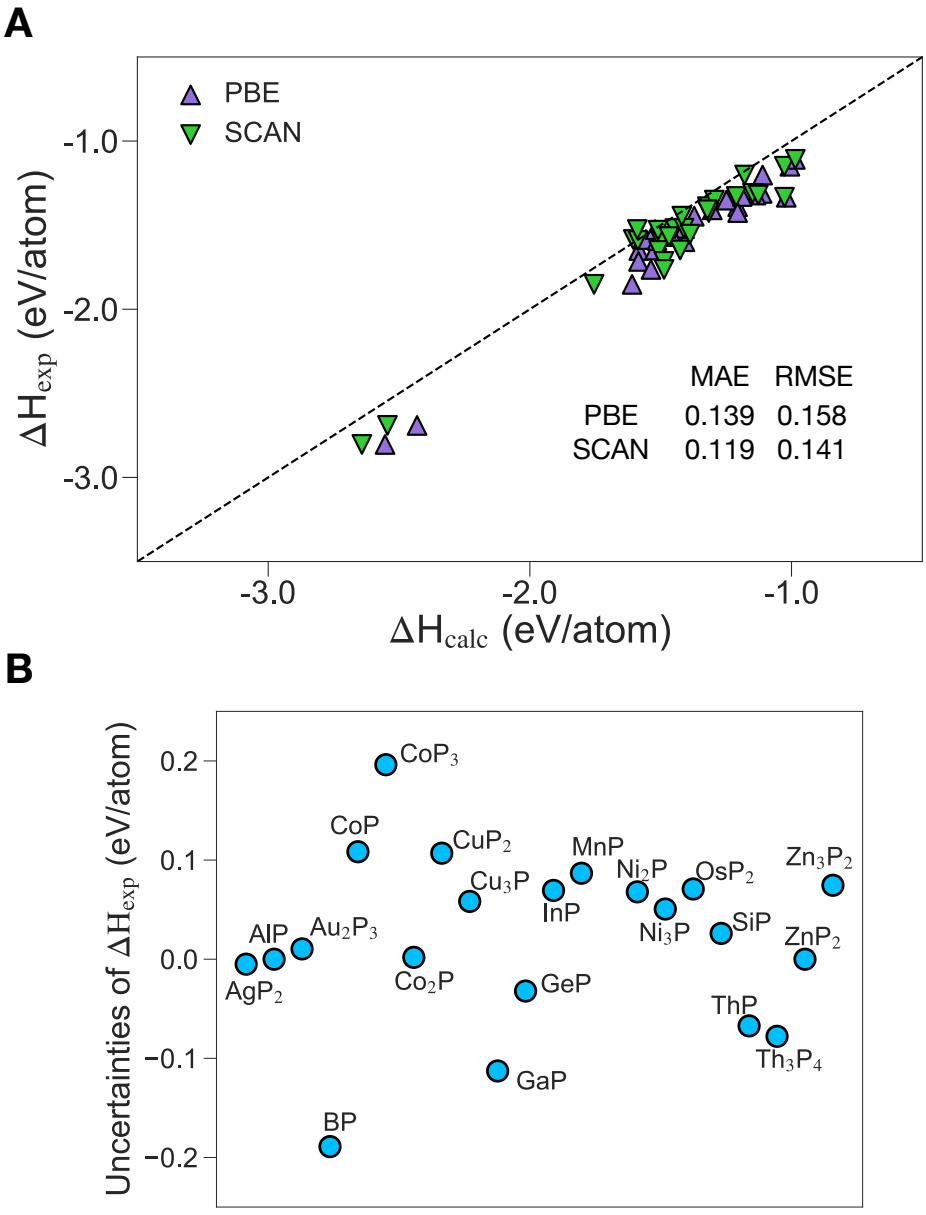

Figure S5: (A) Experimental formation enthalpies (ΔH_{exp}) of 28 binary phosphides as a function of calculated formation enthalpies (ΔH_{calc}). ΔH_{calc} using the PBE functional were retrieved from the Materials Project.[5,16] and ΔH_{exp} were obtained from Ref 17,18. Raw data are provided in Table S2. (B) Uncertainties of ΔH_{exp} between experimental data from 17,18 and 19.

Ni-Mo Pourbaix diagram

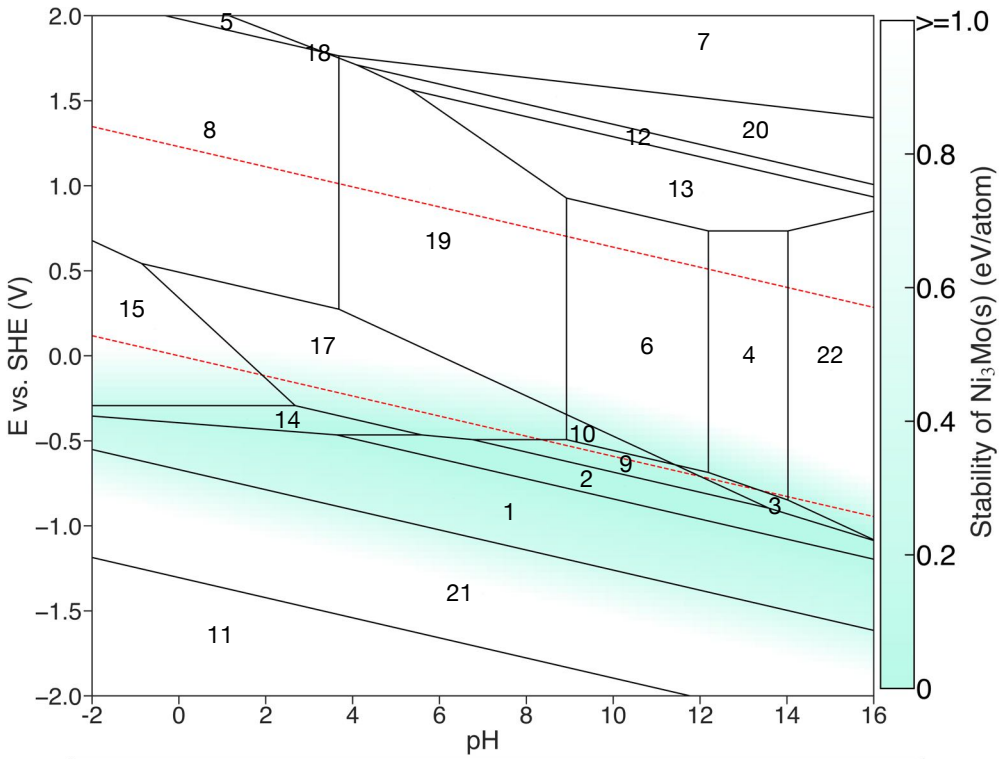

Figure S6: SCAN-calculated Ni-Mo Pourbaix diagrams generated with aqueous ion concentration of 10^{-6} M at 25°C. The blue color measures the stability of Ni_3Mo at relevant potential and pH. The deeper the blue, the more stable of Ni_3Mo. The water stability window is shown in red dashed line.

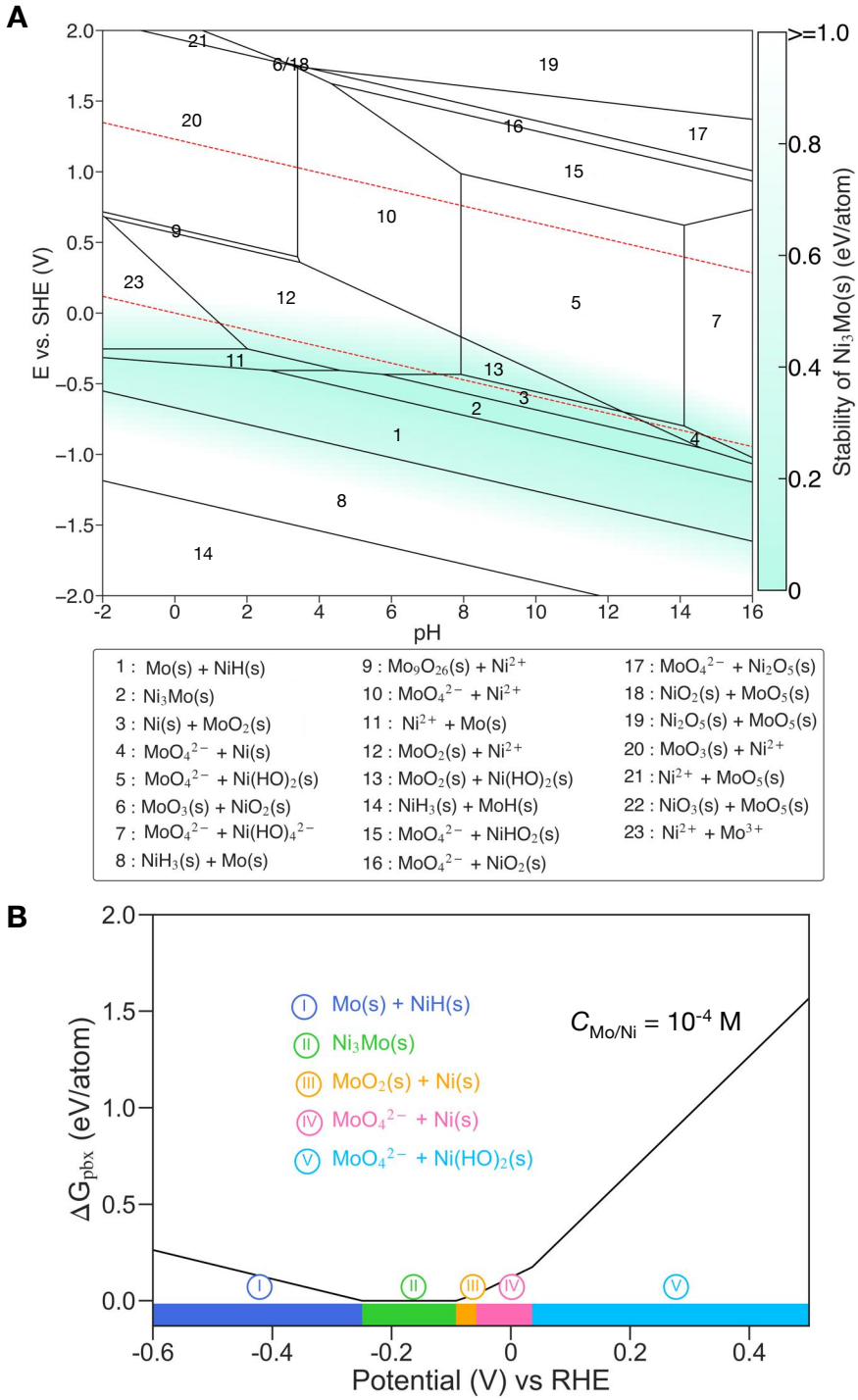

Figure S7: (A) Calculated Ni-Mo Pourbaix diagrams generated with aqueous ion concentration of 10^{-4} M at 25°C. The blue color measures the stability of Ni_3Mo at relevant potential and pH. The water stability window is shown in red dashed line. (B) Calculated Pourbaix decomposition free energy ΔG_{pbx} of Ni_3Mo from the potential -0.6−0.5 V *vs*. RHE at pH = 14. The projection of ΔG_{pbx} onto the potential axis highlights the stable species at the corresponding regions

X-ray powder diffraction of MoP and CoP

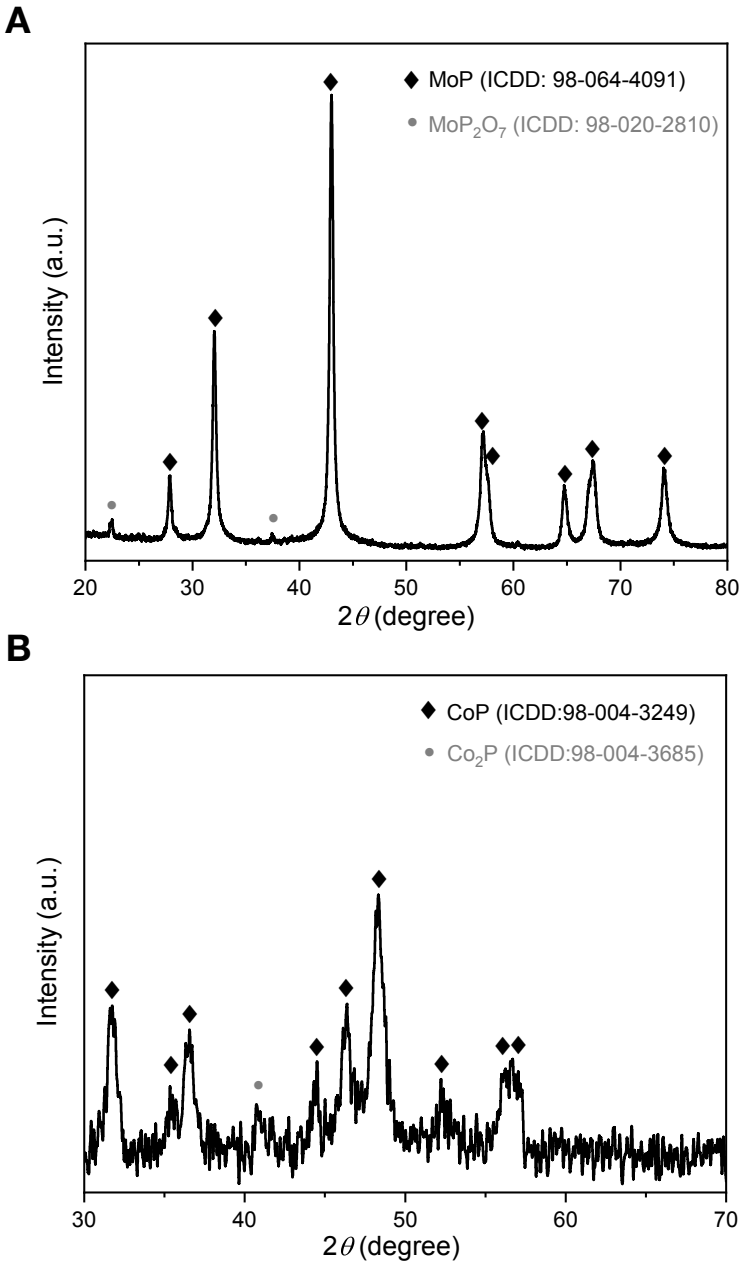

Figure S8: (A) X-ray diffraction pattern of the prepared MoP. The diffraction peaks can be assigned to hexagonal MoP (ICDD: 98-064-4091) (B) X-ray diffraction pattern of the prepared CoP. The diffraction peaks can be assigned to orthorhombic CoP (ICDD: 98-004-3249).

Stability measurement protocol

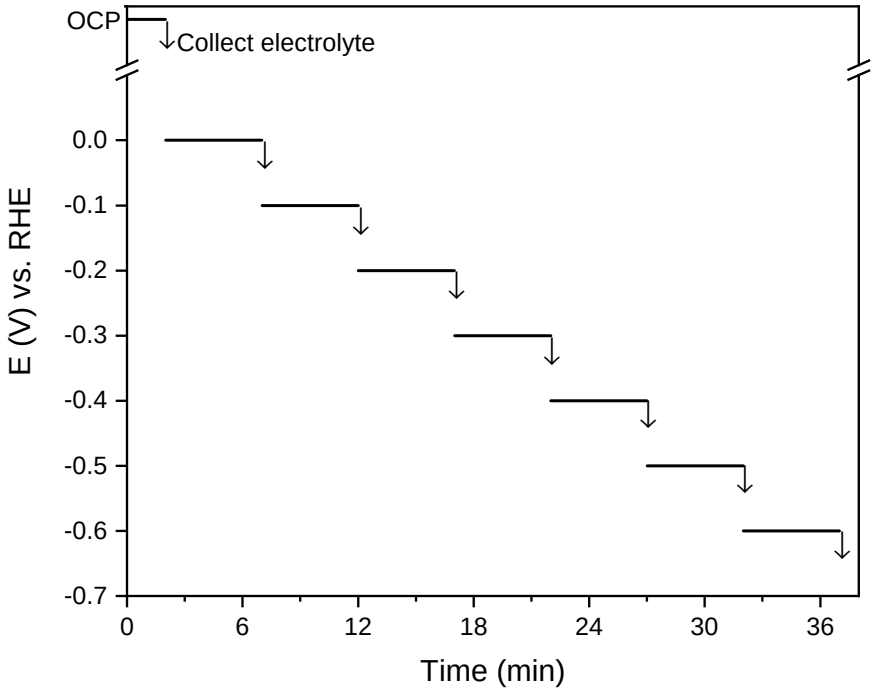

Figure S9: Electrochemical stability measurement protocol of non-precious HER catalysts. The total volume of the electrolyte was 30 mL 0.5 M H_2SO_4. During the measurements, 1 mL of the electrolyte was collected after each potential holding for further ICP-MS analysis.

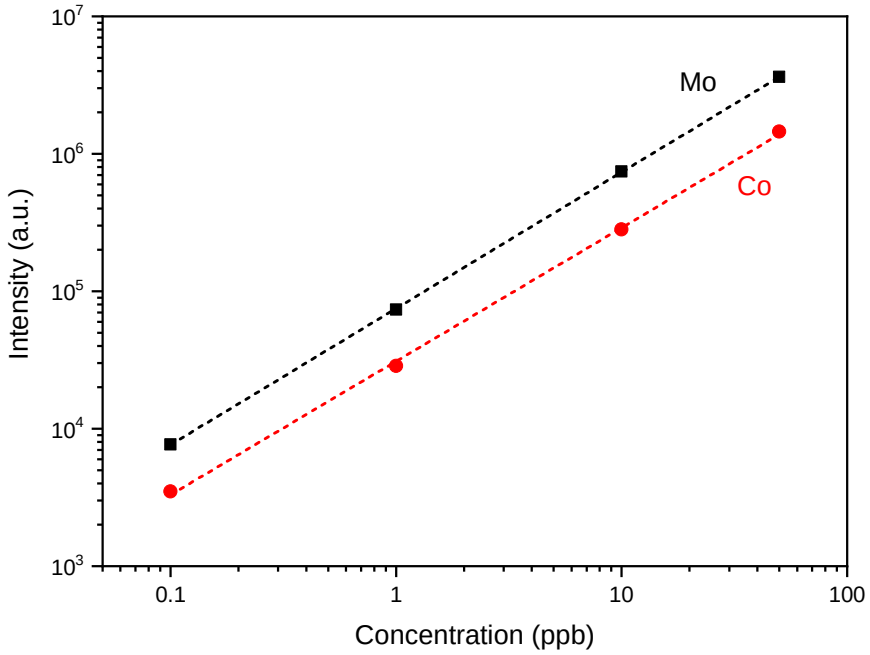

Figure S10: Representative calibration curves for Mo and Co quantification using ICP-MS.

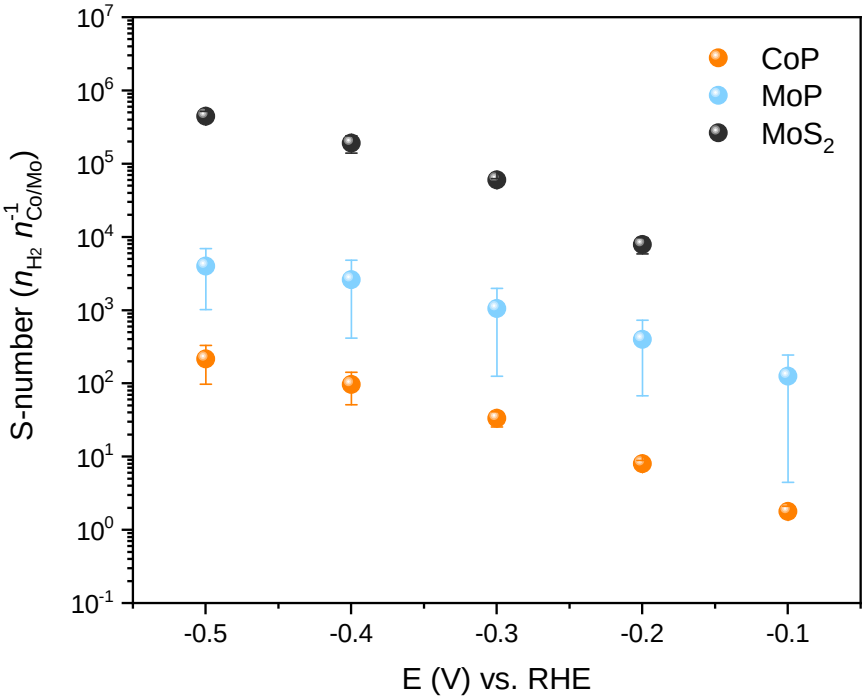

Figure S11: Calculated S-numbers of CoP, MoP, and MoS_2 at different working potentials in 0.5 M H2SO4.

Raw data of calculated and experimental formation enthalpies for 83 sulfides and 28 phosphides

Table S1: Calculated and experimental formation enthalpies (eV/atom) of 83 sulfides. ΔH_{SCAN} and ΔH_{PBE} are calculated data using the SCAN and PBE functional, respectively. ΔH_{MP-PBE} represents PBE calculated data with a sulfur correction of 0.66 eV/S.[20] Both PBE and MP-PBE data were retrieved from the MP.[5,16] The experimental data were obtained from Ref 17,18.

Materials	ΔH_{exp}	ΔH_{SCAN}	ΔH_{MP-PBE}	ΔH_{PBE}	Compound	ΔH_{exp}	ΔH_{SCAN}	ΔH_{MP-PBE}	ΔH_{PBE}
Ag_2S	-0.11	-0.08	-0.276	-0.055	MoS_2	-0.954	-0.928	-1.309	-0.866
Al_2S_3	-1.5	-1.259	-1.455	-1.057	Na_2S	-1.265	-1.259	-1.292	-1.07
As_2S_3	-0.347	-0.173	-0.526	-0.128	NaS	-1.029	-0.992	-1.164	-0.832
AsS	-0.368	-0.167	-0.466	-0.134	Nd_2S_3	-2.333	-2.367	-2.457	-2.059
B_2S_3	-0.523	-0.538	-0.832	-0.434	NdS	-2.409	-2.275	-2.356	-2.024
BaS	-2.402	-2.367	-2.41	-2.079	Ni_3S_2	-0.448	-0.401	-0.636	-0.371
BeS	-1.214	-1.252	-1.388	-1.057	Ni_3S_4	-0.446	-0.474	-0.751	-0.372
Bi_2S_3	-0.297	-0.297	-0.742	-0.344	NiS	-0.456	-0.43	-0.69	-0.359
CS_2	0.308	0.285	-0.172	0.27	OsS_2	-0.508	-0.438	-0.799	-0.357
CaS	-2.452	-2.434	-2.483	-2.151	P_2S_3	-0.251	-0.202	-0.561	-0.163
CdS	-0.774	-0.758	-0.972	-0.641	P_4S_3	-0.333	-0.151	-0.431	-0.146
Ce_2S_3	-2.463	-2.352	-2.425	-2.027	PbS	-0.51	-0.553	-0.865	-0.533
Ce_3S_4	-2.447	-2.302	-2.403	-2.024	Pd_4S	-0.143	-0.197	-0.313	-0.18
CeS	-2.366	-2.216	-2.378	-2.046	PdS	-0.366	-0.479	-0.686	-0.354
Co_3S_4	-0.532	-0.555	-0.817	-0.438	PdS_2	-0.27	-0.357	-0.713	-0.271
CoS	-0.43	-0.423	-0.742	-0.41	PrS	-2.342	-2.278	-2.347	-2.016
CoS_2	-0.529	-0.496	-0.774	-0.331	PtS	-0.431	-0.568	-0.737	-0.406
CrS	-0.819	-0.849	-0.581	-0.25	PtS_2	-0.383	-0.522	-0.792	-0.349
Cs_2S	-1.198	-1.243	-1.18	-0.959	Rb_2S	-1.248	-1.187	-1.215	-0.993
Cu_2S	-0.275	-0.169	-0.346	-0.125	ReS_2	-0.617	-0.581	-1.011	-0.569

Continued on next page

Table S1 – *Continued from previous page*

Materials	ΔH_{exp}	ΔH_{SCAN}	ΔH_{MP-PBE}	ΔH_{PBE}	Compound	ΔH_{exp}	ΔH_{SCAN}	ΔH_{MP-PBE}	ΔH_{PBE}
CuS	-0.271	-0.257	-0.525	-0.194	Rh_2S_3	-0.545	-0.633	-0.869	-0.471
EuS	-2.342	-2.423	-2.47	-2.138	Rh_3S_4	-0.53	-0.619	-0.863	-0.484
FeS	-0.527	-0.474	-0.839	-0.507	RuS_2	-0.711	-0.678	-0.992	-0.55
FeS_2	-0.593	-0.594	-0.955	-0.513	SO_3	-1.136	-1.214	-1.755	-1.062
Ga_2S_3	-1.07	-0.75	-1.06	-0.662	Sb_2S_3	-0.425	-0.255	-0.647	-0.249
GaS	-1.084	-0.711	-0.983	-0.652	SiS_2	-0.737	-0.753	-1.119	-0.677
GeS	-0.394	-0.251	-0.585	-0.253	SmS	-2.234	-2.252	-2.355	-2.023
GeS_2	-0.542	-0.366	-0.769	-0.327	Sn_2S_3	-0.546	-0.431	-0.801	-0.403
HgS	-0.276	-0.176	-0.459	-0.128	SnS	-0.559	-0.444	-0.778	-0.446
In_2S_3	-0.737	-0.706	-0.931	-0.533	SnS_2	-0.531	-0.424	-0.823	-0.381
InS	-0.694	-0.66	-0.823	-0.491	SrS	-2.45	-2.439	-2.475	-2.144
Ir_2S_3	-0.517	-0.452	-0.764	-0.366	TaS_2	-1.223	-1.127	-1.491	-1.048
IrS_2	-0.46	-0.485	-0.843	-0.401	Th_2S_3	-2.245	-2.157	-2.353	-1.954
K_2S	-1.301	-1.247	-1.276	-1.055	ThS	-2.071	-1.962	-2.168	-1.837
KS	-1.12	-1.097	-1.264	-0.932	ThS_2	-2.168	-2.241	-2.427	-1.985
La_2S_3	-2.454	-2.504	-2.591	-2.192	TiS	-1.41	-1.627	-1.8	-1.468
LaS	-2.448	-2.412	-2.495	-2.163	TiS_2	-1.406	-1.475	-1.715	-1.273
Li_2S	-1.544	-1.542	-1.557	-1.336	Tl_2S	-0.328	-0.443	-0.565	-0.344
MgS	-1.792	-1.667	-1.759	-1.428	WS_2	-0.896	-0.825	-1.261	-0.819
MnS	-1.11	-1.03	-0.883	-0.551	ZnS	-1.063	-0.933	-1.144	-0.812
MnS_2	-0.715	-0.801	-0.997	-0.554	ZrS_2	-1.995	-1.771	-1.956	-1.514
Mo_2S_3	-0.844	-0.761	-1.082	-0.684					

Table S2: Calculated and experimental formation enthalpies (eV/atom) of 28 phosphides. ΔH_{SCAN} and ΔH_{PBE} are calculated data using the SCAN and PBE functional, respectively. PBE data were retrieved from the MP.[5,16] The experimental data were obtained from Ref 17,19

Materials	ΔH_{exp}	ΔH_{SCAN}	ΔH_{PBE}	Compound	ΔH_{exp}	ΔH_{SCAN}	ΔH_{PBE}
AgP_2	-0.15	-0.028	-0.006	GeP	-0.109	0.015	0.015
AlP	-0.852	-0.755	-0.609	InP	-0.39	-0.322	-0.206
Au_2P_3	-0.202	-0.18	-0.11	Mn_2P	-0.591	-0.587	-0.514
BP	-0.598	-0.498	-0.407	MnP	-0.585	-0.605	-0.556
Co_2P	-0.648	-0.426	-0.523	Ni_2P	-0.568	-0.468	-0.478
CoP	-0.65	-0.508	-0.584	Ni_3P	-0.519	-0.411	-0.441
CoP_3	-0.53	-0.51	-0.497	NiP_2	-0.447	-0.419	-0.372
Cu_3P	-0.334	-0.027	-0.02	NiP_3	-0.409	-0.322	-0.303
CuP_2	-0.311	-0.149	-0.112	P_2Os	-0.526	-0.589	-0.521
Fe_2P	-0.554	-0.388	-0.458	SiP	-0.321	-0.127	-0.136
Fe_3P	-0.425	-0.316	-0.206	Th_3P_4	-1.691	-1.544	-1.431
FeP	-0.715	-0.488	-0.585	ThP	-1.804	-1.642	-1.553
FeP_2	-0.763	-0.487	-0.537	Zn_3P_2	-0.33	-0.211	-0.188
GaP	-0.52	-0.446	-0.409	ZnP_2	-0.351	-0.295	-0.249

Table S3: Calculated and experimental formation Gibbs free energies (eV/formula) of solids and aqueous ions for SCAN-calculated Pourbaix diagrams. The referenced solids of each Pourbaix diagram are highlighted in bold. The experimental data were obtained from Ref 15,21.

Species	ΔG_{exp}	ΔG_{calc}	Species	ΔG_{exp}	ΔG_{calc}
Mo	-	0	H_2PO_4[-]	-11.715	-
Mo_9O_{26}	-	-59.749	$H_3P_2O_7$[-]	-20.971	-
MoH	-	1.304	H_3PO_4(aq)	-11.842	-
MoO_2	-5.524	-5.456	$H_4P_2O_7$(aq)	-21.061	-
MoO_3	-	-6.779	HP_2O_7[3-]	-20.441	-
MoO_4[2-]	-8.667	-8.599	HPO_3[2-]	-8.412	-
MoO_5	-	-3.920	HPO_4[2-]	-11.289	-
MoS_2	-	-2.784	$P(HO_2)_2$[-]	-	-11.608
Mo[3+]	-0.593	-0.525	**P_2O_5**	-14.114	-13.900
Na_2SO_4	-13.253	-13.085	P_2O_7[4-]	-19.893	-
H_2S(aq)	-0.285	-0.117	P_2O_9	-	-8.603
$H_2S_2O_3$(aq)	-5.551	-	PH_2O_3[-]	-	-8.668
$H_2S_2O_4$(aq)	-6.393	-	PH_3	-	1.091
$H_2S_2O_7$	-	-10.017	PH_3(aq)	0.263	0.370
H_2SO_4(aq)	-7.718	-7.550	PH_3O_4(aq)	-	-11.735
H_2SO_5	-	-5.876	PH_4[+]	0.954	1.061
H_3S	-	0.107	PHO_3[2-]	-	-8.305
HS_2O_3[-]	-5.516	-	PHO_4[2-]	-	-11.182
HS_2O_4[-]	-6.371	-	PO_4[3-]	-10.555	-10.447
HSO_3[-]	-5.469	-	Co	-	0
HSO_4[-]	-7.836	-7.667	$Co(HO)_2$	-	-5.020
HSO_5[-]	-6.607	-6.439	Co_2P	-	-1.277

Continued on next page

Table S3 – *Continued from previous page*

Species	ΔG_{exp}	ΔG_{calc}	Species	ΔG_{exp}	ΔG_{calc}
HS[-]	0.126	0.294	Co_3O_4	-	-8.858
S	-	0	$Co_3P_2(HO)_{16}$	-	-45.586
S_2O_3[2-]	-5.371	-	CoH	-	0.379
S_2O_4[2-]	-6.219	-	CoH_3	-	1.875
S_2O_5[2-]	-8.192	-	$CoHO_2$	-	-4.277
S_2O_6[2-]	-10.014	-	$CoHO_2$[-]	-	-3.855
S_2O_8[2-]	-11.506	-	**CoO**	-2.125	-2.382
S_2[2-]	0.829	-	CoO_2	-	-2.008
S_3O_6[2-]	-9.927	-	CoO_4	-	3.433
S_3[2-]	0.767	-	CoP	-	-1.016
S_4O_6[2-]	-10.588	-	Co[2+]	-0.555	-0.812
S_4[2-]	0.720	-	Co[3+]	1.253	0.996
S_5O_6[2-]	-9.901	-	$HCoO_2$[-]	-3.598	-
S_5[2-]	0.690	-	Ni	-	0
SO_2(aq)	-3.114	-	$Ni(HO)_2$	-4.696	-4.848
SO_3[2-]	-4.949	-4.780	$Ni(HO)_3$[-]	-	-6.231
SO_4	-	-2.217	$Ni(HO)_4$[2-]	-	-7.860
SO_4[2-]	-7.714	-7.545	**$Ni(OH)_2$**	-4.696	-4.848
S[2-]	0.894	1.063	$Ni(OH)_2$(aq)	-4.208	-
H_3Pt	-	2.595	$Ni(OH)_3$[-]	-6.079	-
H_4Pt	-	2.101	$Ni(OH)_4$[2-]	-7.709	-
H_8PtO_6	-	-6.507	Ni_2O_5	-	-1.580
HPt_3	-	2.185	Ni_3Mo	-	-0.166
Pt	0	0	NiH	-	0.195

Continued on next page

Table S3 – *Continued from previous page*

Species	ΔG_{exp}	ΔG_{calc}	Species	ΔG_{exp}	ΔG_{calc}
Pt_2O	-	0.631	NiH_3	-	1.534
Pt_3O_4	-	-3.626	$NiHO_2$	-	-3.393
PtO	-	-0.532	NiO(aq)	-1.706	-
PtO_2	-	-1.651	NiO_2	-	-1.513
PtO_3	-	-0.249	NiO_2[2-]	-2.784	-2.935
PtO_6	-	1.279	NiO_3	-	2.158
Pt[2+]	1.925	1.925	NiOH[+]	-2.355	-
$H_2P_2O_7$[2-]	-20.842	-	Ni[2+]	-0.480	-0.631
H_2PO_3[-]	-8.775	-	-	-	-

References

(1) Kresse, G.; Furthmüller, J. Efficient iterative schemes for *ab initio* total-energy calculations using a plane-wave basis set. *Physical Review B* **1996**, *54*, 11169–11186.

(2) Blöchl, P. E. Projector augmented-wave method. *Physical Review B* **1994**, *50*, 17953–17979.

(3) Sun, J.; Ruzsinszky, A.; Perdew, J. Strongly Constrained and Appropriately Normed Semilocal Density Functional. *Physical Review Letters* **2015**, *115*, 036402.

(4) Jain, A.; Ong, S. P.; Hautier, G.; Chen, W.; Richards, W. D.; Dacek, S.; Cholia, S.; Gunter, D.; Skinner, D.; Ceder, G.; Persson, K. A. Commentary: The materials project: A materials genome approach to accelerating materials innovation. *APL Materials* **2013**, *1*, 011002.

(5) Ong, S. P.; Richards, W. D.; Jain, A.; Hautier, G.; Kocher, M.; Cholia, S.; Gunter, D.; Chevrier, V. L.; Persson, K. A.; Ceder, G. Python Materials Genomics (pymatgen): A robust, open-source python library for materials analysis. *Computational Materials Science* **2013**, *68*, 314–319.

(6) Persson, K. A.; Waldwick, B.; Lazic, P.; Ceder, G. Prediction of solid-aqueous equilibria: Scheme to combine first-principles calculations of solids with experimental aqueous states. *Physical Review B* **2012**, *85*, 235438.

(7) Singh, A. K.; Zhou, L.; Shinde, A.; Suram, S. K.; Montoya, J. H.; Winston, D.; Gregoire, J. M.; Persson, K. A. Electrochemical Stability of Metastable Materials. *Chemistry of Materials* **2017**, *29*, 10159–10167.

(8) Patel, A. M.; Nørskov, J. K.; Persson, K. A.; Montoya, J. H. Efficient Pourbaix diagrams of many-element compounds. *Physical Chemistry Chemical Physics* **2019**, *21*, 25323–25327.

(9) Wang, Z.; Guo, X.; Montoya, J.; Nørskov, J. K. Predicting aqueous stability of solid with computed Pourbaix diagram using SCAN functional. *npj Computational Materials* **2020**, *6*, 160.

(10) Bertheussen, E.; Hogg, T. V.; Abghoui, Y.; Engstfeld, A. K.; Chorkendorff, I.; Stephens, I. E. L. Electroreduction of CO on Polycrystalline Copper at Low Overpotentials. *ACS Energy Letters* **2018**, *3*, 634–640.

(11) Hinnemann, B.; Moses, P. G.; Bonde, J.; Jørgensen, K. P.; Nielsen, J. H.; Horch, S.; Chorkendorff, I.; Nørskov, J. K. Biomimetic Hydrogen Evolution: MoS_2 Nanoparticles as Catalyst for Hydrogen Evolution. *Journal of the American Chemical Society* **2005**, *127*, 5308–5309.

(12) Jaramillo, T. F.; Jørgensen, K. P.; Bonde, J.; Nielsen, J. H.; Horch, S.; Chorkendorff, I. Identification of active edge sites for electrochemical H2 evolution from MoS_2 nanocatalysts. *Science* **2007**, *317*, 100–102.

(13) Chen, Z.; Cummins, D.; Reinecke, B. N.; Clark, E.; Sunkara, M. K.; Jaramillo, T. F. Core–shell MoO_3-MoS_2 Nanowires for Hydrogen Evolution: A Functional Design for Electrocatalytic Materials. *Nano Letters* **2011**, *11*, 4168–4175.

(14) Ledendecker, M.; Mondschein, J. S.; Kasian, O.; Geiger, S.; Göhl, D.; Schalenbach, M.; Zeradjanin, A.; Cherevko, S.; Schaak, R. E.; Mayrhofer, K. Stability and Activity of Non-Noble-Metal-Based Catalysts Toward the Hydrogen Evolution Reaction. *Angewandte Chemie - International Edition* **2017**, *56*, 9767–9771.

(15) Pourbaix, M. *Atlas of Electrochemical Equilibria in Aqueous Solutions.*, 2nd ed.; National Association of Corrosion Engineers: Houston, TX, 1974.

(16) Ong, S. P.; Cholia, S.; Jain, A.; Brafman, M.; Gunter, D.; Ceder, G.; Persson, K. A. The Materials Application Programming Interface (API): A simple, flexible and efficient API for materials data based on REpresentational State Transfer (REST) principles. *Computational Materials Science* **2015**, *97*, 209–215.

(17) O. Kubaschewski; C. B. Alcock; P. J. Spencer, *Materials thermochemistry*, 6th ed.; Pergamon Press, Oxford, NY, 1993.

(18) Linstrom, P.J.; Mallard, W.G., *Eds., NIST Chemistry WebBook, NIST Standard Reference Database Number 69*; National Institute of Standards and Technology, Gaithersburg MD, 20899, https://doi.org/10.18434/T4D303, 2020.

(19) Barin, I. *Thermochemical Data of Pure Substances*, 3rd ed.; Wiley, New York, USA, 1995.

(20) Zhu, Z.; Chu, I.-H.; Deng, Z.; Ong, S. P. Role of Na^+ Interstitials and Dopants in Enhancing the Na^+ Conductivity of the Cubic Na_3PS_4 Superionic Conductor. *Chemistry of Materials* **2015**, *27*, 8318–8325.

(21) Wagman, D. D.; Evans, W. H.; Halow, I.; Parker, V. B.; Bailey, S. M.; Schumm, R. H.; (U.S.), I. f. B. S.; of Standards, U. S. N. B.; of Commerce, U. S. D. *Selected Values of Chemical Thermodynamic Properties*; NBS technical note; United States Department of Commerce, National Bureau of Standards, Washington, D.C., 1966.